Corrugated megathrust revealed offshore Costa Rica

Joel H. Edwards*[1], Jared W. Kluesner[2], Eli A. Silver[1], Emily E. Brodsky[1], Daniel S. Brothers[2], Nathan L. Bangs[3], James D. Kirkpatrick[4], Ruby Wood[1], Kristina Okamoto[1]

[1]Department of Earth and Planetary Sciences, University of California, Santa Cruz, Santa Cruz, California 95064, USA

[2]Pacific Coastal and Marine Science Center, US Geological Survey, Santa Cruz, California 95060, USA

[3]Institute for Geophysics, University of Texas at Austin, PRC 196, 10100 Burnett Rd., Austin TX, USA

[4]Earth and Planetary Sciences, McGill University, 3450 University Avenue, Montreal, Quebec H3A 0E8, Canada

Exhumed faults are rough, often exhibiting topographic corrugations oriented in the direction of slip; such features are fundamental to mechanical processes that drive earthquakes and fault evolution. However, our understanding of corrugation genesis remains limited due to a lack of *in situ* observations at depth, especially at subducting plate boundaries. Here we present 3D seismic reflection data of the Costa Rica subduction zone that image a shallow megathrust fault characterized by (1) corrugated and (2) chaotic and weakly corrugated topographies. The corrugated surfaces extend from near the trench to several km down dip, exhibit high reflection

amplitudes (consistent with high fluid content/pressure) and trend 11–18° oblique to subduction, suggesting 17 – 27 mm/yr of trench-parallel slip partitioning across the plate boundary. The corrugations form along portions of the megathrust with greater cumulative slip and may act as fluid conduits. In contrast, weakly corrugated areas occur adjacent to active plate bending faults where the megathrust has migrated up-section, forming a nascent fault surface. The variations in megathrust roughness imaged here suggest that abandonment and then reestablishment of the megathrust up-section transiently increases fault roughness. Analogous corrugations may exist along significant portions of subduction megathrusts globally.

Faults at field and laboratory scales are observed to be non-planar, or rough, and at earthquake scales (kilometers), are inferred to be irregular and heterogenous[1–4]. Exhumed fault surfaces commonly display corrugations or striations parallel to the slip direction[5,6] that are observed across a broad range of spatial scales[7,8] (µm to km), mechanical media, and geologic environments[9–12]. For example, slip corrugations are observed along the interfaces between fast-flowing ice streams and underlying sediments[11,13]. The mechanical processes proposed for corrugation formation are diverse, including: asperity ploughing and abrasion, debris streaking, and fracture/fault branching and linkage, among others[14–16]. Despite a general recognition that corrugations play a fundamental role in the behavior of faults, to our knowledge, well-defined corrugations have not been observed *in situ* at seismogenic depths along a fault surface, including across an interface of subducting tectonic plates.

The recent 2011 M_w 9 Tohoku-Oki earthquake demonstrated that coseismic slip can propagate all the way to the trench, and that maximum slip can occur along the shallowest portions of the megathrust[17]. Subsequent work has shown that ruptures propagate farther along smoother faults due to smaller stress heterogeneity[18] and fewer adjacent fracture networks available for off-fault slip[19]. Thus, greater fault roughness is thought to inhibit rupture propagation and has been inferred to do so offshore Costa Rica, where a zone of seamounts, plateaus and ridges are subducting, and the earthquake record lacks evidence for historic shallow coseismic slip[20,21,19]. We map with unprecedented spatial resolution the shallow 3D megathrust offshore Costa Rica and demonstrate *in situ* heterogeneity in the fault structure.

Megathrust morphology from 3D seismic reflection data

Here we utilize a 2011 3D depth-migrated seismic reflection volume offshore the Osa Peninsula of southern Costa Rica[22,23], along the northwest portion of the Cocos Ridge, where the Cocos Plate dives below the Caribbean Plate. The 3D volume images the megathrust at 12.5 x 18.75 m horizontal resolution (binning size) and ~5 – 15 m shallow vertical resolution[24]. Within the depth-migrated volume we mapped the megathrust (Figures 1-2) utilizing post stack processing, filtering[25] and amplitude-driven tracking techniques[26] commonly used in oil and gas exploration. The megathrust was differentiated by both its polarity and structural position, namely that it either separates landward-dipping reflections from underlying subhorizontal reflections or that it cuts across and through landward-dipping reflections (Figure 2b-e). We corroborate this interpreter-driven result with independently derived volumetric attributes, such as apparent dip[27] and curvature[28], that extract subtle geometric variations of features from trace to trace to better constrain the detailed megathrust morphology (Figure 3). The resulting surface is the best-resolved 3D perspective of any shallow megathrust to date. It reveals a plate interface with remarkable detail and contrasts, varying from 1) smooth and well-developed to 2) rough and weakly-developed (Figures 1-3). Furthermore, the smooth and well-developed portions are corrugated, with corrugations that are meters to tens of meters high, extend kilometers along their long axes (length) and hundreds of meters across their short axes (width). The corrugated portions also exhibit high reflector amplitudes and reversed polarity relative to the seafloor (Figure 1-4).

The corrugations are observed within hundreds of meters (>200-600 m) from the up-dip extent of the megathrust and can be seen extending down-dip >5 km to plate bending faults (~1.4 km below seafloor; Figures 2-3). At these shallow depths, corrugation distribution is heterogenous with the shallow central and eastern portions of the megathrust having a relatively chaotic morphology that lacks well-defined corrugations (Figures 1-3). These shallow chaotic portions generally coincide with places where the megathrust has propagated up section (relative to its original position) through tilted, fractured and consolidated strata of the frontal prism[29,30], capturing upper plate material and transferring it to the subducting plate (frontal prism erosion; Figure 2b, d and e). These newly propagated portions of the megathrust spatially coincide with large-offset (~>200 m) plate bending faults, either propagating down dip for landward-dipping faults or up dip for seaward-dipping faults (Figure 2). Several local plate bending faults seem to be propagating into the overlying frontal prism, possibly due to delayed initial plate bending that is landward of the trench rather than seaward of the trench. In contrast, normal faults are typically first observed at the outer rise, i.e., outer trench wall, along other Pacific convergent margins[31] (Figure 2). Newly propagated portions of the megathrust generally form proximal to plate bending faults with offsets ~>200 m, although an exception is within the most SE portion, where trench-parallel offsets are <200 m, even down to <100 m. This exception could be due to lateral propagation (along strike) of the new megathrust from the central area. Regardless, because these newer portions of the megathrust have accommodated small amounts of slip, they have not developed a well-defined surface, resulting in lower amplitude and relatively chaotic seismic reflections (Figure 2). These portions lack well-defined corrugations (Figures 1-3).

Scale of corrugations

We extracted corrugation widths and heights across the megathrust horizon. The corrugations have a median width and height of 160 m and 7 m, with a range of 113 – 729 m and 2.7 – 53 m (Figure 4). The corrugations are at a similar scale to structures along other large-scale displacement interfaces, including intermediate-scale corrugations along onshore and offshore low-angle detachments faults[9,10,32,33] and mega-scale glacial lineations[11]. A best fit linear trend to the data gives a height/width aspect ratio of 0.08. This value of 0.08 is slightly larger than observed for terrestrial fault exposures[16], although it may be biased high because of detectability limitations[34]. Heights less than the theoretical vertical resolution of ~5 m are observable due to the 3D nature of the data. In this case, the corrugations generally extend hundreds of meters to kilometers, extending beyond the Fresnel zone (horizontal resolution), making heights <5 m detectable. Figure 4 reports heights as low as 2.7 m. These values indicate that significant height corrugations exist that could be important for producing seismic waves, channeling fluids and controlling tremor locations as inferred from previous studies of exhumed faults[8,16,35].

Corrugation genesis

We observe several consistencies with outcrop fault corrugations[5–8]. The corrugations are not imaged along underthrusting, undeformed strata or in the overlying frontal prism (Figure 2b-e). The corrugations do not coincide with truncations and/or offset of reflections below or above the megathrust (i.e., are not coincident with trench perpendicular faulting; Figure 2b-e). Furthermore, they are oriented ~11 – 18˚ clockwise from plate motion vectors[36,37], making them more orthogonal to the trench and more closely aligned with regional earthquake slip vectors[38]. Based on these observations, and in conjunction with their continuity, distribution and scale, we interpret the corrugations to be non-penetrative slip lineations that form due to slip along the plate interface.

What slip processes drive their formation is less clear. We have imaged discrete features (we call knobs in Figures 1-3) that are at a similar scale as most of our observed corrugations (Figure 4). These knobs could act as asperities that groove or furrow adjacent rock, analogous to groove-ploughing theories[14,15]; however, they lack detectable corrugations in their wake (Figure 2). Alternatively, could processes thought to control meter-scale roughness, such as anastomosing and linking slip surfaces that form lenses[16], scale up to these hundreds of meters wide corrugations? Detailed 3D imaging of *in situ* corrugations observed here extend those observed at outcrop scales and those observed along other mechanical media and provide a new dataset for future quantitative investigations.

Implications for forearc translation

Previous work has shown compelling evidence for strain partitioning along the Costa Rica margin[38,39], resulting in a forearc that is being translated predominantly northwestward (trench parallel). Using the orientation of two prominent troughs from the NW and SE megathrust as slip directions, and MORVEL plate velocities[36,37], we constrain the rate of northwestward translation offshore Osa to ~17 – 27 mm/yr (Figure 3d). These rates are higher than previous rates of 11 – 17 mm/yr from Costa Rica to Guatemala[37,38]. We also observe a relatively continuous counter-clockwise rotation of slip, ~7˚, from the southeastern to northwestern portion (away from the Cocos Ridge), ~11 km along strike (Figures 2-3). The counter-clockwise rotation fits the regional trend of rotation of slip away from the Cocos Ridge, as seen in slope seamount scars and GPS derived velocity fields[39]. Our observed counter-clockwise rotation of slip and lower trench parallel rates away from the Cocos Ridge support the model of the Cocos Ridge acting as a rigid indenter that drives tectonic escape and trench parallel motion[37,39], even in areas where convergence is nearly orthogonal (southern Costa Rica).

Implications for earthquakes

These new observations demonstrate several important processes. They show that the megathrust is smoothed as it accumulates slip (i.e., matures), aligning with results seen in outcrop[40], and that slip develops corrugations at similar scales to corrugations seen along exhumed faults in other environments[9,10,32,33].The well corrugated portions produce notably higher amplitude negative polarity reflections, which have been linked to higher fluid content in these environments[23]. Furthermore, within these fluid-rich corrugated portions, we observe streaks of low amplitudes (Figure 3c), which correspond to troughs of larger individual corrugations (e.g., Troughs NW and SE; Figure 2b and 2c).

These observations, coupled with findings from offshore Nicoya[30], suggest that as fluids ascend to, or move along, the nonplanar and corrugated megathrust, they are bounded by its low cross-fault permeability and thus migrate from local lows (troughs) to local highs (ridges). This could facilitate linear zones of varying pore-fluid pressures from troughs to ridges, which have been appealed to at greater depths in prior work related to slip-parallel streaking of tremor[35].

It is not clear whether historical earthquakes offshore Costa Rica have slipped to the trench (e.g., 1983 Osa Earthquake M_w=7.4[41]). However, well recorded earthquakes, like the 2012 Nicoya Earthquake M_w=7.6 or the 2002 Osa Earthquake M_w=6.4 (nucleated only at ~6 km depth and ~25 km from the trench), do not seem to have done so[20,42]. Our data show that the shallow, smooth and corrugated portions of the megathrust are bordered by younger and rougher generations of the megathrust cutting through the base of the overlying plate. If rougher and/or immature faults inhibit rupture propagation[18,19], our data may show why deeper coseismic slip offshore Costa Rica does not propagate to the trench and why earthquakes there seem to have multiple rupture patches[19]. Furthermore, because continued plate bending faulting with subduction is seen at other convergent margins[43], our results provide a means to assess the tendency for shallow coseismic slip elsewhere.

Novel technology and workflows[25–28] applied to a 3D pre-stack depth-migrated volume of a subduction zone have made it possible to document *in situ* corrugations along a megathrust within an active subduction zone for the first time. These findings also have important implications for the net exchange of materials under the frontal prism and more broadly the exchange of material at a margin thought to be erosive. Finally, because corrugations are observed across the entire width of the 3D volume, we speculate that analogous corrugations exist along portions of subduction megathrusts globally. The previous hypotheses proposing that corrugations control slip and fluid behavior on the plate interface appear to be well-founded[35,44].

References

1. Aki, K. Asperities, Barriers, Characteristic Earthquakes and Strong Motion Prediction. *J. Geophys. Res.* **89,** 5867–5872 (1984).
2. Scholz, C. H. The mechanics of earthquakes and faulting. *Cambridge Univ. Press* 496 (2002).
3. Shi, Z. & Day, S. M. Rupture dynamics and ground motion from 3-D rough-fault simulations. *J. Geophys. Res.* **118,** 1122–1141 (2013).
4. Dieterich, J. H. & Smith, D. E. Nonplanar Faults: Mechanics of Slip and Off-fault Damage. *Pure appl. Geophys.* **166,** 1799–1815 (2009).
5. Petit, J. P. Criteria for the sense of movement on fault surfaces in brittle rocks. *J. Struct. Geol.* **9,** 597–608 (1987).
6. Engelder, J. T. Microscopic Wear Grooves on Slickensides: Indicators of Paleoseismicity. *J. Geophys. Res.* **79,** 4387–4392 (1974).
7. Candela, T. & Brodsky, E. E. The minimum scale of grooving on faults. *Geology* 1–4 (2016). doi:10.1130/G37934.1
8. Kirkpatrick, J. D. & Brodsky, E. E. Slickenline orientations as a record of fault rock rheology. *Earth Planet. Sci. Lett.* **408,** 24–34 (2014).
9. Wright, L. A., Otton, J. K. & Troxel, B. W. Turtleback Surfaces of Death Valley

Viewed as Phenomena of Extensional Tectonics. *Geology* 53–54 (1974).

10. John, B. E. Geometry and evolution of a mid-crustal extensional fault system: Chemehuevi Mountains, southeastern California. *Geol. Soc. London Spec. Publ.* **28,** 313–334 (1987).

11. Clark, C. D. Mega-scale glacial lineations and cross-cutting ice-flow landforms. *Earth Surf. Process. Landforms* **18,** 1–29 (1993).

12. Cann, J. R. *et al.* Corrugated slip surfaces formed at ridge-transform intersections on the Mid-Atlantic Ridge. *Nature* **385,** 329–332 (1997).

13. King, E. C., Hindmarsh, R. C. a. & Stokes, C. R. Formation of mega-scale glacial lineations observed beneath a West Antarctic ice stream. *Nat. Geosci.* **2,** 585–588 (2009).

14. Means, W. D. A newly recognized type of slickenside striation. *J. Struct. Geol.* **9,** 585–590 (1987).

15. Clark, C. D., Tulacyzk, S., Stokes, C. R. & Canals, M. A groove-ploughing theory for the production of mega-scale glacial lineations, and implications for ice-stream mechanics. *J. Glaciol.* **49,** 240–256 (2003).

16. Brodsky, E. E., Kirkpatrick, J. D. & Candela, T. Constraints from fault roughness on the scale-dependent strength of rocks. *Geology* **44,** 1–4 (2016).

17. Lay, T., Ammon, C. J., Kanamori, H., Xue, L. & Kim, M. J. Possible large near-trench slip during the 2011 Mw 9.0 off the Pacific coast of Tohoku Earthquake. *Earth, Planets Sp. Lett.* **63,** 687–692 (2011).

18. Bletery, Q. *et al.* Mega-earthquakes rupture flat megathrusts. *Science (80-.).* **354,** 1027–1031 (2016).

19. Wang, K. & Bilek, S. L. Do subducting seamounts generate or stop large earthquakes? *Geology* **39,** 819–822 (2011).

20. Chaves, E. J., Duboeuf, L., Schwartz, S. Y., Lay, T. & Kintner, J. Aftershocks of the 2012 Mw 7.6 Nicoya, Costa Rica, earthquake and mechanics of the plate interface. *Bull. Seismol. Soc. Am.* **107,** 1227–1239 (2017).

21. DeShon, H. R. *et al.* Seismogenic zone structure of the southern Middle America Trench, Costa Rica. *J. Geophys. Res.* **108,** (2003).

22. Kluesner, J. W. *et al.* High density of structurally controlled, shallow to deep water fluid seep indicators imaged offshore Costa Rica. *Geochemistry, Geophys. Geosystems* **14,** 519–539 (2013).

23. Bangs, N. L., McIntosh, K. D., Silver, E. A., Kluesner, J. W. & Ranero, C. R. Fluid accumulation along the Costa Rica subduction thrust and development of the seismogenic zone. *J. Geophys. Res.* **120,** 67–86 (2014).

24. Kallweit, R. S. & Wood, L. C. The limits of resolution of zero-phase wavelets. *Geophysics* **47,** 1035 (1982).

25. Chopra, S. & Marfurt, K. J. Preconditioning seismic data with 5D interpolation for computing geometric attributes. *Interpret. Corner* 1456–1459 (2013).

26. Tingdahl, K. M. & de Groot, P. Post-stack dip- and azimuth processing. *J. Seism. Explor.* **12,** 113–126 (2003).

27. Marfurt, K. J. Robust estimates of 3D reflector dip and azimuth. *Geophysics* **71,** P29–P40 (2006).

28. Roberts, A. Curvature Attributes and their Application to 3D Interpreted Horizons. *First Break* **19,** 85–100 (2001).

29. Harris, R. N., Sakaguchi, A., Petronotis, K. & Scientists, I. E. 344 S. Frontal prism Site U1412. *Integr. Ocean Drill. Progr.* **344,** 1–62 (2013).

30. Tobin, H. J., Vannucchi, P. & Meschede, M. Structure, inferred mechanical properties, and implications for fluid transport in the decollement zone, Costa Rica convergent margin. *Geology* **29,** 907–910 (2001).

31. Masson, D. G. Fault patterns at outer trench walls. *Mar. Geophys. Res.* **13,** 209–225 (1991).

32. Tucholke, B. E., Lin, J. & Kleinrock, M. C. Megamullions and mullion structure defining oceanic metamorphic core complexes on the Mid-Atlantic Ridge. *J. Geophys. Res.* **103,** 9857–9866 (1998).

33. Dinter, D. A. Late Cenozoic extension of the Alpine collisional orogen , northeastern Greece : Origin of the north Aegean basin. *GSA Bull.* **110,** 1208–1226 (1998).

34. Rafaelsen, B. *et al.* Geomorphology of buried glacigenic horizons in the Barents Sea from three-dimensional seismic data. *Geol. Soc. Am. Spec. Publ.* **203,** 259–276 (2002).

35. Ghosh, A. *et al.* Rapid, continuous streaking of tremor in Cascadia. *Geochemistry Geophys. Geosystems* **11,** 1–10 (2010).

36. Demets, C., Gordon, R. G., Argus, D. F. & Stein, S. Geologically current plate motions. *Geophys. J. Int.* **181,** 1–80 (2010).

37. Kobayashi, D. *et al.* Kinematics of the western Caribbean: Collision of the Cocos Ridge and upper plate deformation. *Geochemistry, Geophys. Geosystems* 1671–1683 (2014). doi:10.1002/2014GC005234.Received

38. DeMets, C. A new estimate for present-day Cocos-Caribbean plate motion: Implications for slip along the Central American volcanic arc. *Geophys. Res. Lett.* **28,** 4043–4046 (2001).

39. LaFemina, P. C. *et al.* Fore-arc motion and Cocos Ridge collision in Central America. *Geochemistry, Geophys. Geosystems* **10,** (2009).

40. Sagy, A., Brodsky, E. E. & Axen, G. J. Evolution of fault-surface roughness with slip. *Geology* **35,** 283–286 (2007).

41. Adamek, S. & Tajima, F. Seismic rupture associated with subduction of the Cocos Ridge. *Tectonics* **6,** 757–774 (1987).

42. Arroyo, I. G., Grevemeyer, I., Ranero, C. R. & von Huene, R. Interplate seismicity at the CRISP drilling site: The 2002 Mw 6.4 Osa Earthquake at the southeastern end of the Middle America Trench. *Geochemistry Geophys. Geosystems* **15,** 3035–3050 (2014).

43. Isacks, B. & Molnar, P. Mantle Earthquake Mechanisms and the Sinking of the Lithosphere. *Nature* **223,** 1121–1124 (1969).

44. Rubin, A. M., Gillard, D. & Got, J. Streaks of microearthquakes along creeping faults. *Nature* **400,** 635–641 (1999).

45. Ryan, W. B. F. *et al.* Global Multi-Resolution Topography synthesis. *Geochemistry Geophys. Geosystems* **10,** 1–9 (2009).

46. Spagnolo, M. *et al.* Size, shape and spatial arrangement of mega-scale glacial lineations from a large and diverse dataset. *Earth Surf. Process. Landforms* **39,** 1432–1448 (2014).

Acknowledgements

This work was supported by US National Science Foundation grants OCE-0851380 and OCE-1154635. We thank dGB Earth Sciences for free access to OpendTect Pro and associated commercial plugins.

Author contributions

J.W.K., E.A.S. and N.L.B. obtained financial support for the marine seismic reflection program and collected and processed the seismic data. J.H.E. applied post processing, performed amplitude-driven tracking and extracted geometric attributes along the shallow megathrust. E.E.B. called attention to the corrugations. D.S.B. and J.D.K. furthered analysis of the corrugations. R.W. and K.O. extracted the scale of the corrugations. J.H.E. wrote the manuscript with contributions from all other authors.

Competing financial interests

The authors declare no competing financial interests.

Figure Captions

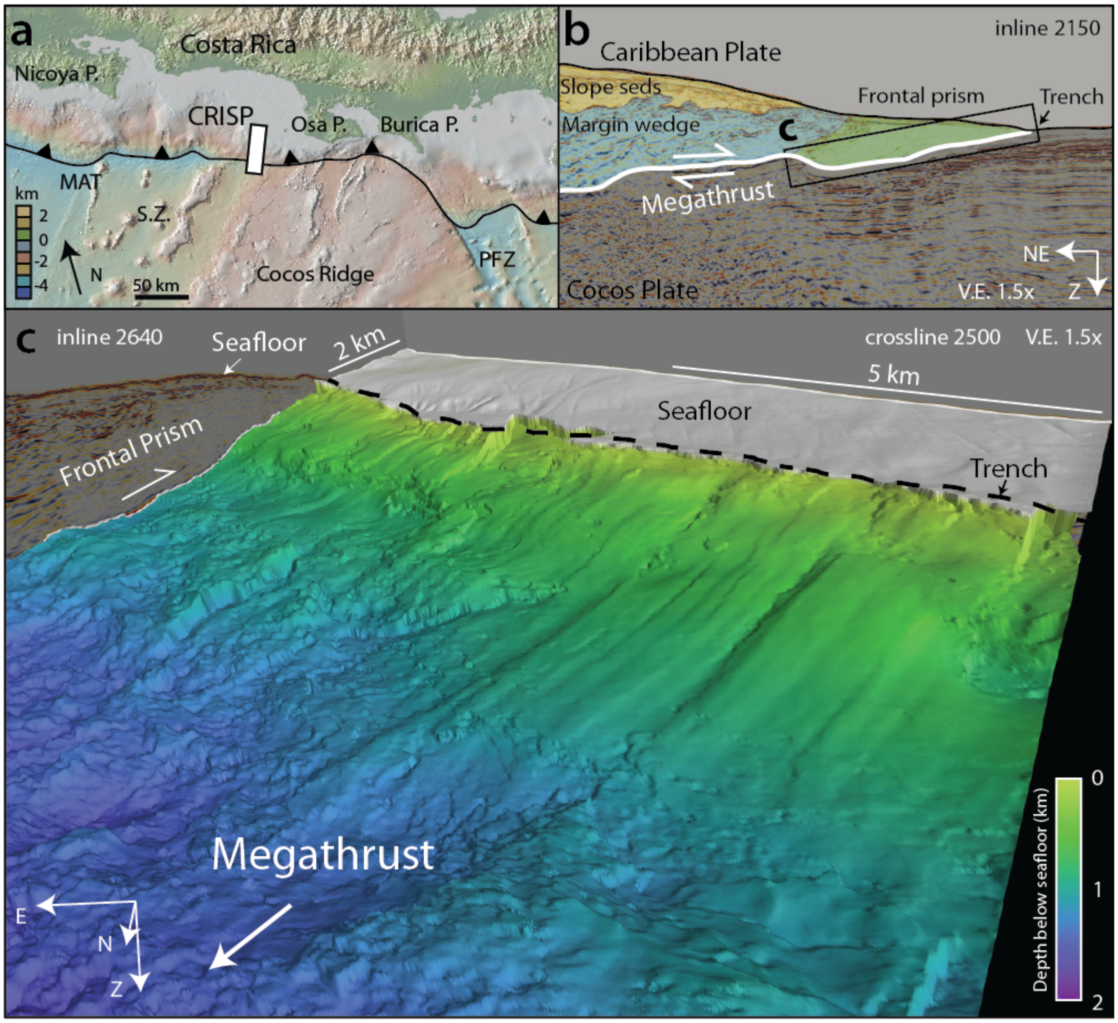

Figure 1 | Tectonic setting, seismic reflection profile and upslope perspective view of the megathrust. a, Topographic shaded relief map of the Costa Rica margin (from Global Multi-Resolution Topography (GMRT) synthesis within GeoMapApp[45]). The Middle American Trench (MAT) is shown with a black line and black triangles on the upper plate. 2011 The coverage of the 3D seismic reflection volume (CRISP) is shown with a white rectangle. **b,** Inline 2150 from the CRISP volume is showing the trench, frontal prism (green) and outer wedge with interpreted sections of slope sediments (yellow) and margin wedge (blue). **c,** Perspective view of the shallow megathrust looking seaward toward the trench and the frontal prism has been cut away. Inline 2640 (frontal prism) is shown for reference. Color scale is kilometers (km) below seafloor and grey denotes the seafloor. V.E. is vertical exaggeration.

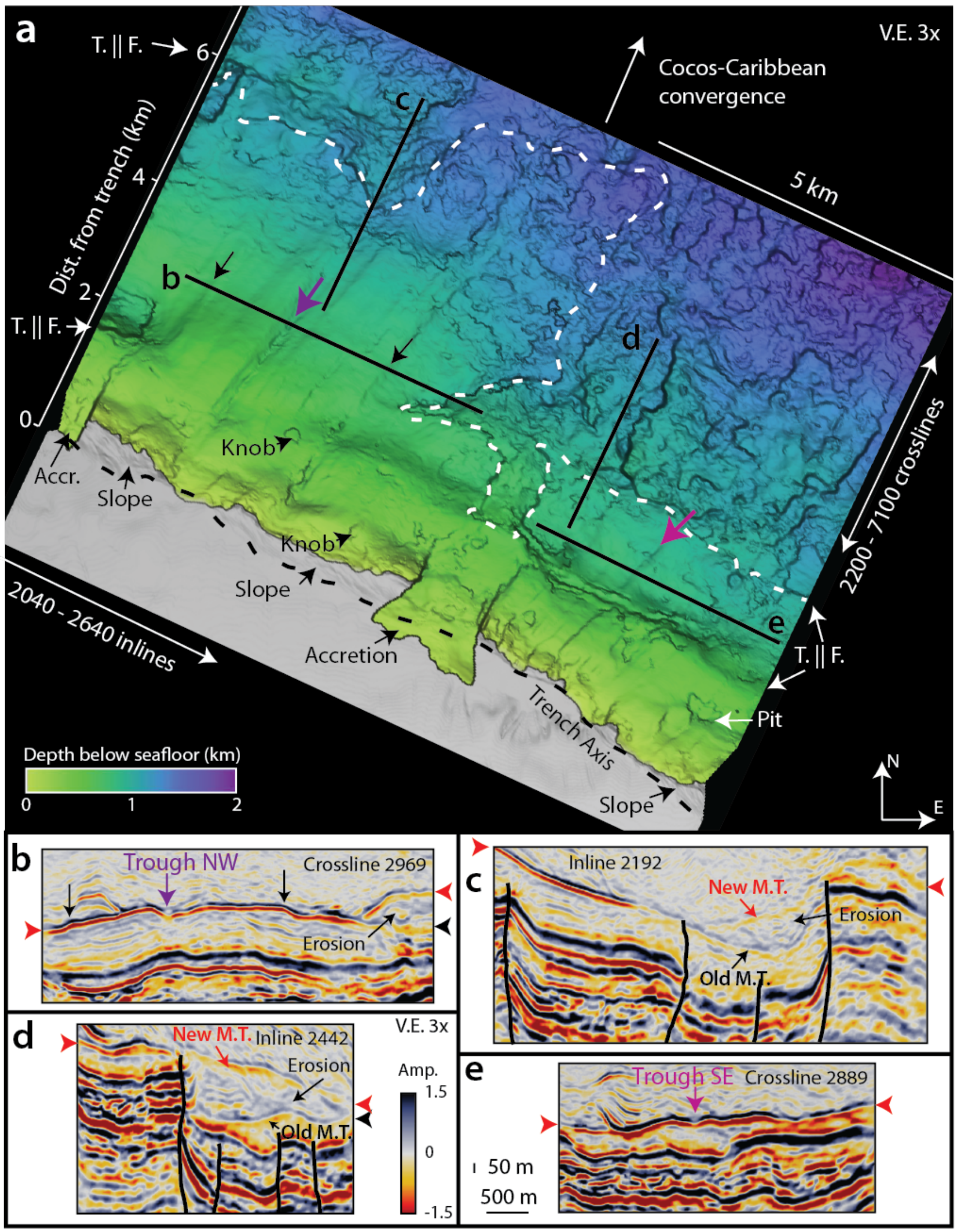

Figure 2 | Map view of depth below seafloor and seismic reflection images of shallow megathrust. a, Map view of shallow megathrust with depth below seafloor (km) overlain in greens (thinner) to blues (thicker). Trench is shown with dashed black line.

Approximate boundary from corrugated to weakly corrugated is shown with dashed white line. Black solid lines denote locations of inlines and crosslines shown in b-e. Inline numbers increase from left to right and crossline numbers increase from bottom to top. Black arrows denote prominent ridges in map view and in b. Purple arrow is prominent trough labeled Trough NW in map view and in b. Pink arrow is Trough SE in map view and in c. T||F is trench parallel faults. **b,** Crossline 2969 showing depth section of corrugated megathrust with prominent troughs (including Trough NW) and ridges. Note low amplitude reflection at center of Trough NW. **c-d,** Inlines 2192 and 2442 showing depth sections of down dip portion of corrugations where the megathrust steps up section in relation to large offset trench parallel faults (shown with white dashed lines). **e,** Crossline 2889 showing depth section of corrugations within the southeast portion, including Trough SE. Amplitude reflection color scale and vertical and horizontal scale is shown between panels d and e. M.T. is megathrust. Red arrowheads denote active megathrust and black arrowheads denote former megathrust Note change of megathrust reflection amplitude along well corrugated versus weakly corrugated portions.

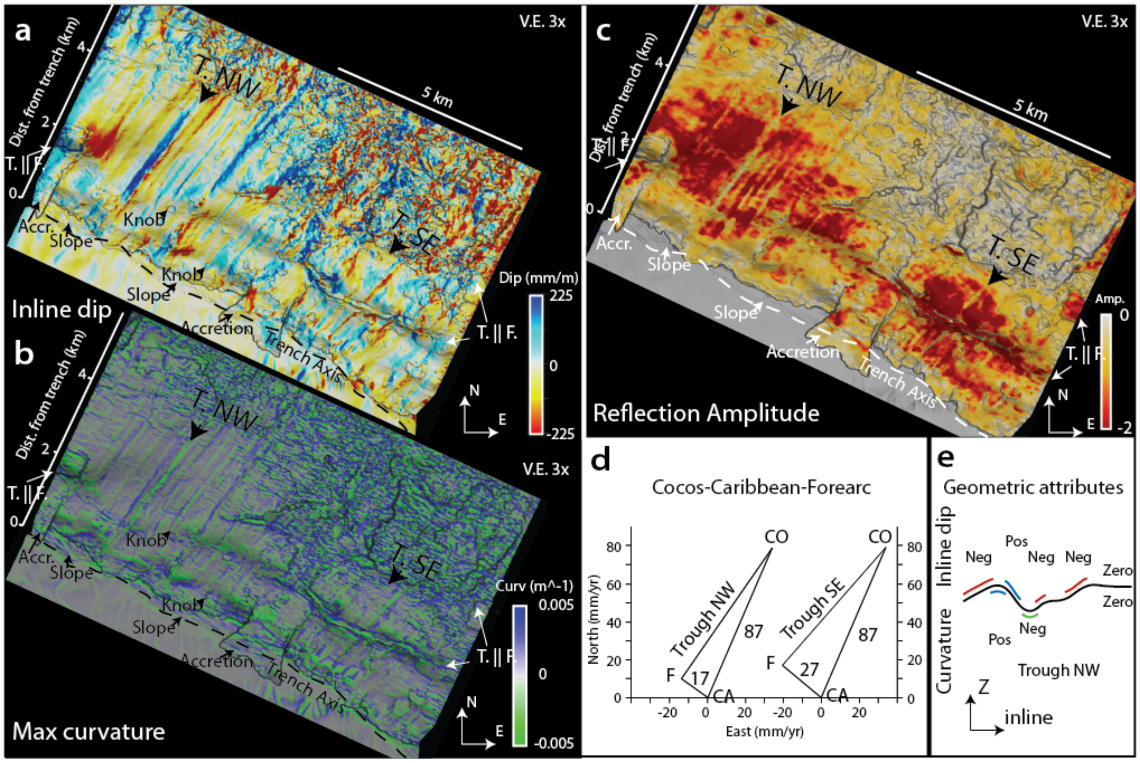

Figure 3 | Map view of dip, curvature and reflection amplitude along megathrust, linear velocity diagram and a reference dip/curvature diagram. a-c, Inline dip, maximum curvature and reflection amplitude extracted along the picked megathrust horizon. Note that with inline dip values, blues and reds meet along the axes of troughs and ridges, i.e., inline dip highlights the sides of dipping features. Whereas with maximum curvature, trough and ridge axes are highlighted by greens (troughs) and blues (ridges). Note how sensitive maximum curvature is to more chaotic portions of the megathrust and note linear streaks of low amplitudes along corrugation troughs. **d,** Linear velocity diagram of trench parallel slip from the orientations of Trough NW and Trough SE. CO is Cocos Plate, CA is Carribbean Plate, and F is Forearc. **e,** Reference diagram for inline dip and curvature. For inline dip, blues dip to the SE and reds dip to the NW. For curvature, greens denote troughs and blues denote ridges.

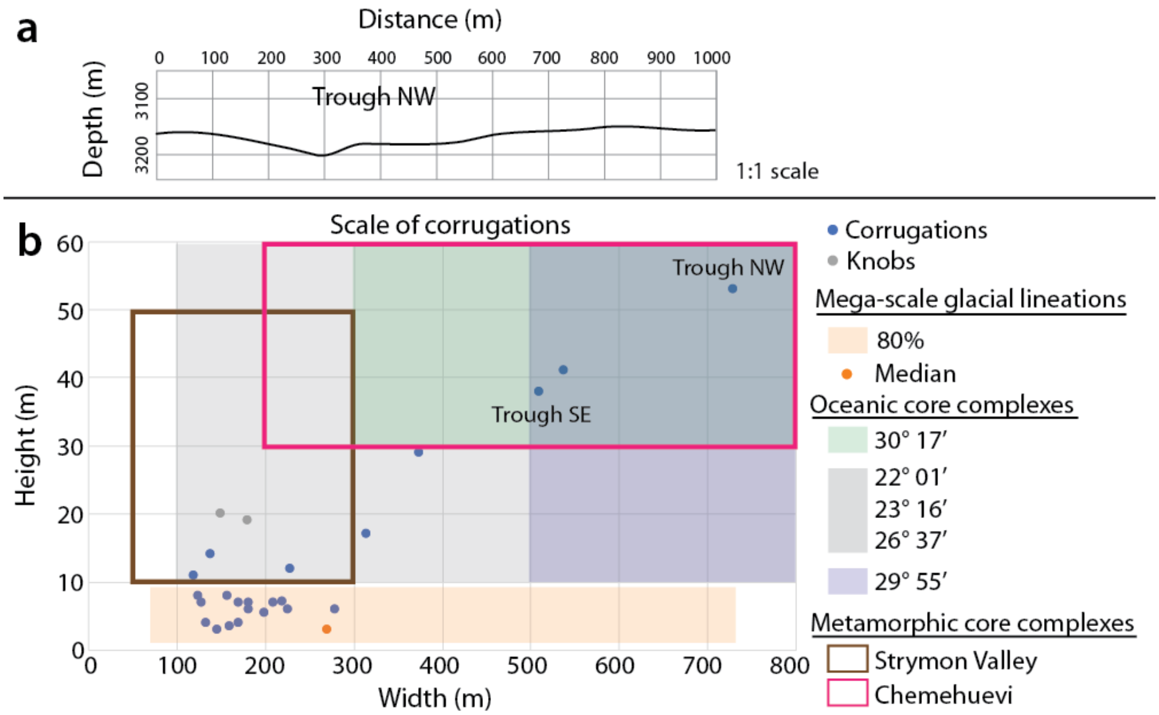

Figure 4 | Scale of corrugations. a, A 1:1 scale of Trough NW for reference. **b,** Widths and heights plotted of corrugations and knobs from megathrust. Overlain are the ranges of corrugations from mega-scale glacial lineations[46] (80% of measurements and median value), oceanic core complexes[32] (intermediate scale) and metamorphic core complexes[10,33].

Methods

3D seismic reflection data. The 3D seismic reflection dataset was acquired aboard the *R/V Marcus G. Langseth* in 2011 using a source of two 27-gun arrays spaced 75 m apart and four 6 km long streamers spaced 150 m apart. The two 27-gun array fired every 25 m in flip-flop mode and had a volumetric displacement of 3200 liters. Each streamer consisted of 468 channels with 12.5 m channel spacing. Data were recorded for 8 s at a 2-ms sample rate. Subsequent processing of the data removed multiples and suppressed noise using normal seismic processing workflows, including: high pass and band pass filtering, noisy trace removal, spherical divergence correction, amplitude gain control, velocity analysis, deconvolution, stacking and a post-stack time migration performed by CGGVeritas and Repsol in Madrid, Spain. These data were then used to generate a 3D velocity model that was utilized in a full pre-stack depth migration performed by Repsol in The Woodlands, TX. The resulting depth-migrated dataset consists of 12.5 x 18.75 m bins with ~60 fold and images the interface between the Cocos and overlying Caribbean plates down to depths >10 km.

Post processing data conditioning. Dip and azimuth data were calculated for every sample along every trace within the volume using the Fast Fourier Transform (FFT) algorithm within OpendTect v6.0.6 software[26]. The FFT iteratively transformed a moving sub-cube of 5x5x5 samples (inlines x crosslines x depth; relative to the sample and trace of interest) into the 3D Fourier Domain and found samples along adjacent traces with the same phase within the designated window. Once adjacent samples with the same phase are found, the apparent dip and azimuth (either inline or crossline direction) are recorded for that sample along that trace. This results in 3D surfaces of constant phase as recorded by a 3D volume of apparent dip and azimuth data, referred to as a steering cube, that should represent apparent geologic structure. This steering cube was then used to guide a 2x2 median filter that smoothed amplitudes and removed noise. With the 2x2 median filtered data, another iteration of FFT 3x3x5 was performed, resulting in a smoother, less noisy steering cube that preserves structure.

Megathrust mapping. Mapping efforts were performed within OpendTect v6.0.6 on the 2x2 median filtered data and were augmented by the FFT 3x3x5 steering cube. Mapping was done using an iterative workflow of interpreter picks and amplitude-driven auto tracking: 1) Pre-load an area of interest with the 2x2 median filtered data, 2) load inlines and crosslines, 3) start/load megathrust horizon, 4) pick several samples along megathrust, termed seeds, that are auto tracked along that inline or crossline, 5) adjust amplitude-driven auto tracking parameters, in this case, we used correlation threshold values that ranged from ~60-95% (algorithm compared the amplitude of the last tracked pick to the next candidate pick), and search windows of ~10-50 m, 6) 3D auto track, 7) QC auto tracked horizon, undo or delete errant portions, adjust picks and/or auto tracking parameters and re-track, 8) lock tracked seeds and repeat. During amplitude-driven tracking, a sub-sample depth value (<5 m) is achieved by fitting a quadratic polynomial to a series of 5 m sample points. Once the megathrust is tracked, the horizon is gridded to fill in remaining holes, using an algorithm that is guided by the steering cube.

Volumetric attributes. Apparent inline and crossline dips were calculated for data conditioning and contained within the steering cube. Positive inline dips are to the SE (increasing inlines) and negative to the NW (decreasing inlines). Positive crossline dips are to the NE (increasing crosslines) and negative crossline dips are to the SW (decreasing crosslines). Maximum curvature is derived from the apparent dip volume contained in the steering cube by using it to estimate local 3D surfaces for each sample in the volume with a 3x3 least squares fit grid. Using these 3x3 surfaces, maximum curvature is calculated for every sample using simple arithmetic approximations and mean and Gaussian curvatures[28].

Measuring corrugations. Geometries were measured manually with graphical tools in Matlab and OpendTect. In Matlab, troughs and ridges were extracted from xyz elevation data using a 20 by 20 element moving window to average all z values within the square neighborhood for every element in the matrix. These neighborhood averaged z values were then subtracted from the original elevation data. The resulting matrix consists of positive values where the central z value is greater than the neighborhood average and negative when less, corresponding to topographic highs and lows respectively. This differencing matrix helped constrain troughs and ridges. The widths of each is determined as the distance from trough to trough or peak to peak, and the amplitudes as the difference in elevation between the peak and trough, as measured graphically in Matlab and OpendTect. In Matlab, widths and amplitudes were extracted along the horizon and in OpendTect, widths and amplitudes were measured along selected crosslines. Measurements in Matlab were corroborated by measurements in OpendTect and vice versa. ~30 total bedforms were measured at discrete points along the megathrust (i.e., a representative part of the corrugation was measured). Two amplitudes <1 m were excluded.